



HAL
open science

Large Deformation Diffeomorphic Metric Mapping and Fast-Multipole Boundary Element Method provide new insights for Binaural Acoustics,

Reza Zolfaghari, Nicolas Epain, Craig Jin, Joan Alexis Glaunès, Anthony Tew

► To cite this version:

Reza Zolfaghari, Nicolas Epain, Craig Jin, Joan Alexis Glaunès, Anthony Tew. Large Deformation Diffeomorphic Metric Mapping and Fast-Multipole Boundary Element Method provide new insights for Binaural Acoustics,. IEEE International Conference on Acoustics, Speech, and Signal Processing, May 2014, Italy. <http://arxiv.org/abs/1401.7100>. hal-01053758

HAL Id: hal-01053758

<https://hal.science/hal-01053758v1>

Submitted on 1 Aug 2014

HAL is a multi-disciplinary open access archive for the deposit and dissemination of scientific research documents, whether they are published or not. The documents may come from teaching and research institutions in France or abroad, or from public or private research centers.

L'archive ouverte pluridisciplinaire **HAL**, est destinée au dépôt et à la diffusion de documents scientifiques de niveau recherche, publiés ou non, émanant des établissements d'enseignement et de recherche français ou étrangers, des laboratoires publics ou privés.

LARGE DEFORMATION DIFFEOMORPHIC METRIC MAPPING AND FAST-MULTIPOLE BOUNDARY ELEMENT METHOD PROVIDE NEW INSIGHTS FOR BINAURAL ACOUSTICS

Reza Zolfaghari, Nicolas Epain, Craig T. Jin, Joan Glaunès, Anthony Tew

ABSTRACT

This paper describes how Large Deformation Diffeomorphic Metric Mapping (LDDMM) can be coupled with a Fast Multipole (FM) Boundary Element Method (BEM) to investigate the relationship between morphological changes in the head, torso, and outer ears and their acoustic filtering (described by Head Related Transfer Functions, HRTFs). The LDDMM technique provides the ability to study and implement morphological changes in ear, head and torso shapes. The FM-BEM technique provides numerical simulations of the acoustic properties of an individual’s head, torso, and outer ears. This paper describes the first application of LDDMM to the study of the relationship between a listener’s morphology and a listener’s HRTFs. To demonstrate some of the new capabilities provided by the coupling of these powerful tools, we examine the classical question of what it means to “listen through another individual’s outer ears.” This work utilizes the data provided by the Sydney York Morphological and Acoustic Recordings of Ears (SYMARE) database.

Index Terms— SYMARE, LDDMM, HRTF, Ear Morphology, Binaural Hearing

1. INTRODUCTION

Morphoacoustic signal processing is a relatively new term in binaural acoustics [1]. It refers to signal processing in which the relationship between a listener’s morphology (the shape of the torso, head, and ears) and the listener’s individualized acoustic filtering properties plays a prominent role. The acoustic filters required for synthesizing high-fidelity 3D audio for an individual listener are referred to as head-related impulse response (HRIR) filters. These filters describe the acoustic filtering properties of the torso, head, and outer ears and how they transform the sound waves that arrive from some location in space, interact with the ear, and ultimately

reach the tympanic membrane. This acoustic filtering imparts a signature to the incoming sound that the human auditory system perceptually decodes as spatial information. The Fourier transform of the HRIR filters are referred to as head-related transfer functions (HRTFs).

The study of the relationship between morphological shape and acoustic filtering has been on-going for over a decade now. For example, [2] applied regression and principle component analysis to establish a linear relation between morphological and acoustic data. In another study, [3] proposed a “best fit” HRTF based on a similarity score between individual anthropometric measurements and data available in the CIPIC database. More recently [1] has characterized the effect of small perturbations on the magnitude of the notches and peaks appearing in the frequency spectrum of a single HRTF. Similar work conducted by [4] investigates the effect of the ear morphology upon the magnitude of the N1 notch in the median plane.

We now briefly introduce the tools that are applied in this study, beginning with the FM-BEM. Traditionally, individual HRTFs are acoustically measured in an anechoic chamber that incorporates a robotic arm to move a sound source in space. Microphones are placed in the ears of the listener and impulse responses are recorded for a number of directions in space. This clearly requires specialized equipment and is time consuming for the listener. With the increasing computational power of personal computers and also the improvement in numerical methods for boundary element method simulations, such as the fast multipole method [5], a listener’s HRTFs can now be numerically derived using acoustic simulations conducted using high-resolution surface meshes of the listener. Considerable research has been done to establish the validity of numerical simulations of HRTFs using the BEM [5, 6, 7]. These research show that high resolution surface meshes of the torso, head and ears are sufficient to provide accurate numerical simulation of HRTFs that provide a reasonable match to the acoustically-measured HRTFs.

We now introduce a shape analysis tool referred to as Large Deformation Diffeomorphic Metric Mapping (LDDMM) [8, 9] that will be used to manipulate and study ear shapes. LDDMM models the mapping of one surface, C , to another surface, S , as a dynamic flow of diffeomorphisms of the ambient space, \mathbb{R}^3 , in which the surfaces are embedded. The computations for LDDMM are not performed directly in

This work was supported by the UK Engineering and Physical Sciences Research Council (grant GR/T28140/01) and the Australian Research Council’s Discovery Projects funding scheme (project number DP110102920).

R. Zolfaghari, N. Epain and C.T. Jin are with CARLab, School of Electrical and Information Engineering, The University of Sydney, Sydney, Australia. email: craig.jin@sydney.edu.au.

A. Tew is with the Department of Electronics, The University of York, Heslington, York, UK. email: tony.tew@york.ac.uk.

J.A. Glaunès is with the MAP5, Université Paris 5-René Descartes, 75006 Paris, France. email: alexis.glaunes@mi.parisdescartes.fr.

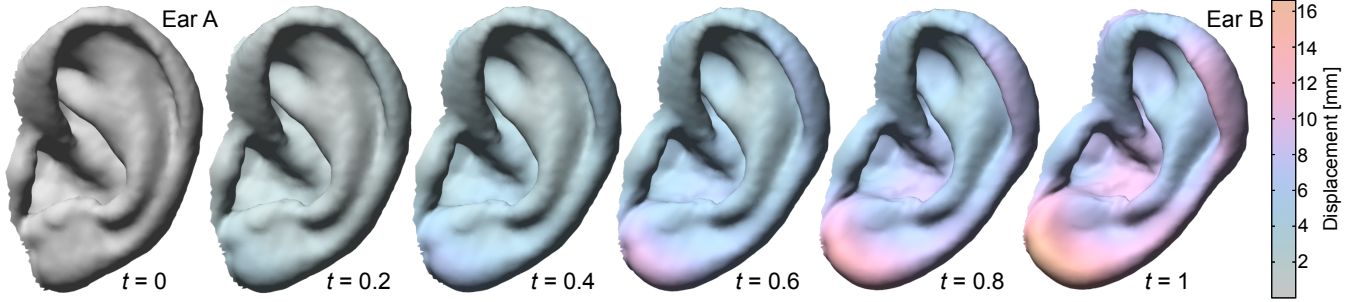


Fig. 1: The result of the flow of diffeomorphisms for several time steps is shown for the matching of Ear A to Ear B. The color indicates cumulative displacement. A constant luminance colormap has been used for best results, so please examine the figure online.

the space of diffeomorphisms; instead, the method works with time dependent vector fields, $\mathbf{v}(t) : \mathbb{R}^3 \rightarrow \mathbb{R}^3$ for $t \in [0, 1]$, which model the infinitesimal efforts of the flow. The flow of diffeomorphisms, $\phi^{\mathbf{v}}(t, X)$, operating on a subset $X \subset \mathbb{R}^3$ is defined via the partial differential equation:

$$\frac{\partial \phi^{\mathbf{v}}(t, \mathbf{X})}{\partial t} = \mathbf{v}(t) \circ \phi^{\mathbf{v}}(t, \mathbf{X}), \quad (1)$$

where \circ denotes the composition of functions. Note that the superscript \mathbf{v} on $\phi^{\mathbf{v}}(t, \mathbf{X})$ has no significance except to denote that the flow of diffeomorphisms is defined for a particular set of time dependent vector fields $\mathbf{v}(t)$.

The diffeomorphism at time $t = 0$, is the identity diffeomorphism: $\phi^{\mathbf{v}}(0, C) = C$. The result of the flow of diffeomorphisms at time $t = 1$ maps C to S : we write this as $\phi^{\mathbf{v}}(t, C)|_{t:[0 \rightarrow 1]} = S$. The time dependent vector fields, $\mathbf{v}(t)$, belong to a Hilbert space of regular vector fields that has a kernel, k_V , and a norm $\|\cdot\|_V$ that models the infinitesimal cost of the flow. In the LDDMM framework, we solve an inexact matching problem which minimizes the cost function, $J_{C,S}$, defined as:

$$J_{C,S}(\mathbf{v}(t)_{t \in [0,1]}) = \gamma \int_0^1 \|\mathbf{v}(t)\|_V^2 dt + E(\phi^{\mathbf{v}}(t, C)|_{t:[0 \rightarrow 1]}, S), \quad (2)$$

where E is a norm-squared cost measuring the degree of matching between $\phi^{\mathbf{v}}(t, C)|_{t:[0 \rightarrow 1]}$ and S . In this work, we use the Hilbert space of currents [10, 11, 12] to compute E because it is easier and more natural than using landmarks.

In order to make the concept of the flow of diffeomorphisms explicit, consider Fig. 1. In this figure, we transform the surface mesh for Ear A to that for Ear B. We show the flow of diffeomorphisms $\phi^{\mathbf{v}}(t, \text{Ear A})|_{t:[0 \rightarrow t_i]}$ for times $t_i = \{0, 0.2, 0.4, 0.6, 0.8, 1.0\}$.

In order to apply the tools of FM-BEM and LDDMM, we use the SYMARE database [6] which provides high-resolution surface meshes of the head and torso both with and without ears. The database also provides high-resolution

surface meshes of the ears alone. The basic idea behind this paper is to manipulate shapes using LDDMM and to examine the resulting acoustics using FM-BEM. The problem that we consider is the classical question of: “what does it mean to listen through another individual’s outer ears.” In examining this question, we demonstrate and validate our approach to combining the tools of LDDMM and FM-BEM. We also reveal an interesting finding regarding the influence of the head and torso on HRTFs. In Section 2 we describe the methods; Section 3 describes the results and Section 4 concludes.

2. METHOD

This study starts with high-resolution surface meshes (approximately 800 K triangular elements) of the torso, head, and ears for two subjects in the SYMARE database, referred to as $S1$ and $S2$ (top row of Fig. 2). The surface meshes are triangulated meshes composed of a collection of vertices, $x_n, 1 \leq n \leq N$, such that $x_n \in \mathbb{R}^3$ and a set of connectivity information for these points, $f_m, 1 \leq m \leq M$, which constitute the triangular faces of the mesh. Note that for simplicity, we use $S1$ and $S2$ to designate both the subjects and their corresponding surface meshes. Using the tools of LDDMM, we apply two shape transformations to the surface mesh for $S1$. In one transformation, we transform the left ear of $S1$ such that it is similar to the left ear of $S2$. The resulting surface mesh is referred to as $S12_{\text{ear-only}}$. In a second transformation, we transform the torso, head, and left ear (but not the right ear) of $S1$ to be similar to the torso, head, and left ear of $S2$. The resulting surface mesh is referred to as $S12_{\text{all}}$. The two shape transformations described above are shown in the bottom row of Fig. 2. We also perform similar shape transformations to $S2$, but in the reverse direction from $S2$ to $S1$, to obtain $S21_{\text{ear-only}}$ and $S21_{\text{all}}$. All together, we have six different surface meshes consisting of the two original surface meshes and the four transformed surface meshes.

In order to describe how the shape transformations are implemented using LDDMM, we define three mathematical operations – *translate*: \mathcal{T} ; *match*: \mathcal{M} ; and *flow*: \mathcal{F} .

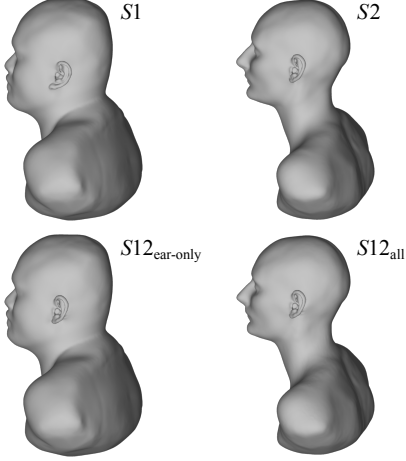


Fig. 2: Surface meshes are shown for $S1$ and $S2$ (top row) and for $S12_{\text{ear-only}}$ and $S12_{\text{all}}$ (bottom row).

The mathematical operation $\mathcal{T}(S1, S2)$ applies a translation to the surface mesh $S1$ such that it best matches surface mesh $S2$. The mathematical operation $\mathcal{M}(S1, S2)$ finds the momentum vectors, $\alpha_n(t)$, that minimize the cost function $J_{S1, S2}(\mathbf{v}(t)_{t \in [0,1]})$. The momentum vectors describe the change to a point, $\mathbf{x}(t)$, in the ambient space, at a given time step via the following differential equation:

$$\frac{d\mathbf{x}(t)}{dt} = \sum_{n=1}^N k_V(\mathbf{x}_n(t), \mathbf{x}) \alpha_n(t), \quad (3)$$

where $k_V(\mathbf{x}, \mathbf{y})$ is the Cauchy kernel defined by:

$$k_V(\mathbf{x}, \mathbf{y}) = \frac{1}{1 + \frac{\|\mathbf{x} - \mathbf{y}\|^2}{\sigma_V^2}}. \quad (4)$$

The parameter σ_V determines the range of influence of the momentum vectors $\alpha_n(t)$. The mathematical operation $\mathcal{F}(S1, \{\alpha\})$ applies the flow of diffeomorphisms defined by a set of momentum vectors, $\{\alpha\}$, to the surface mesh $S1$. For simplicity in this notation, we have not made explicit the time dependence of the momentum vectors, $\{\alpha\}$.

With the definitions of the three mathematical operations (\mathcal{T} , \mathcal{M} , and \mathcal{F}) in hand, it is straightforward to describe the methods to determine $S12_{\text{ear-only}}$ and $S12_{\text{all}}$ from $S1$. Fig. 3 shows and describes the five steps required to synthesize $S12_{\text{ear-only}}$ from $S1$. Fig. 4 shows and describes the three steps required to synthesize $S12_{\text{all}}$ from $S1$. In order to follow the procedures listed in Figs. 3 and 4, it is important to understand that the SYMARE database provides high-resolution surface meshes of the torso and head without ears. So, for example, in Fig. 3 we can learn the momentum vectors required to match $HT1$ (the torso and head surface mesh of $S1$ without ears) to $HT2$ (the torso and head surface mesh of $S2$ without ears). We can then apply this flow of

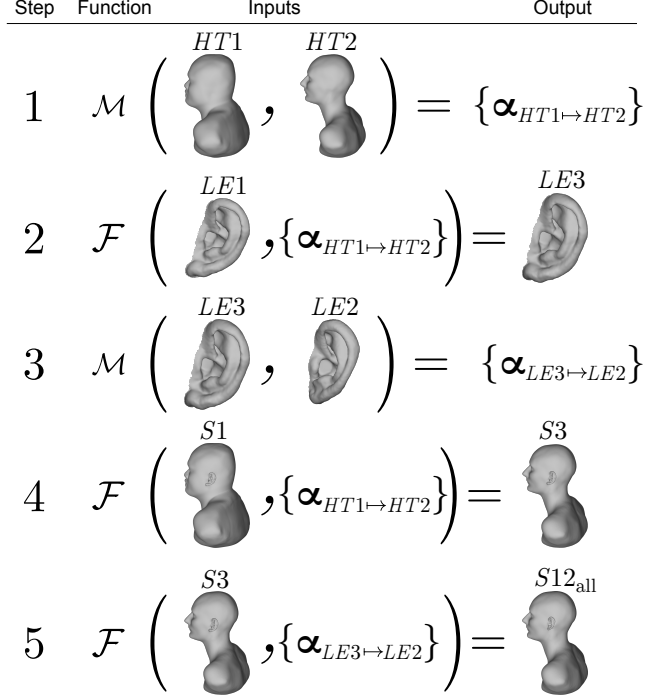


Fig. 3: The steps in the transformation of $S1$ to $S12_{\text{all}}$ are shown.

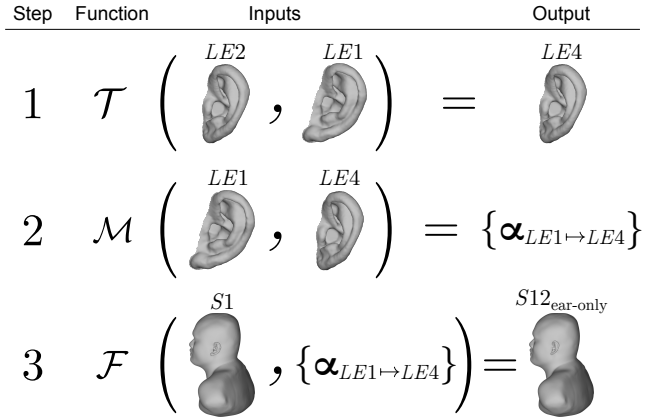


Fig. 4: The steps in the transformation of $S1$ to $S12_{\text{ear-only}}$ are shown.

diffeomorphisms to $LE1$ (the left ear of $S1$) to obtain the intermediate left ear $LE3$. We can then learn the momentum vectors required to match $LE3$ to $LE2$ (the left ear of $S2$). We can then apply both flows of diffeomorphisms sequentially to $S1$ to obtain $S12_{\text{all}}$. Synthesizing $S12_{\text{all}}$ is a control condition in the sense that the HRTFs for $S12_{\text{all}}$ should be identical to that for $S2$. In Fig. 4 we show the steps to obtain $S12_{\text{ear-only}}$. Because the head diameter of $S1$ and $S2$ are not identical, we translate $LE2$ to match $LE1$. We then learn the momentum vectors required to match $LE1$ to the translated version of $LE2$ and apply the flow of diffeomorphisms to $S1$

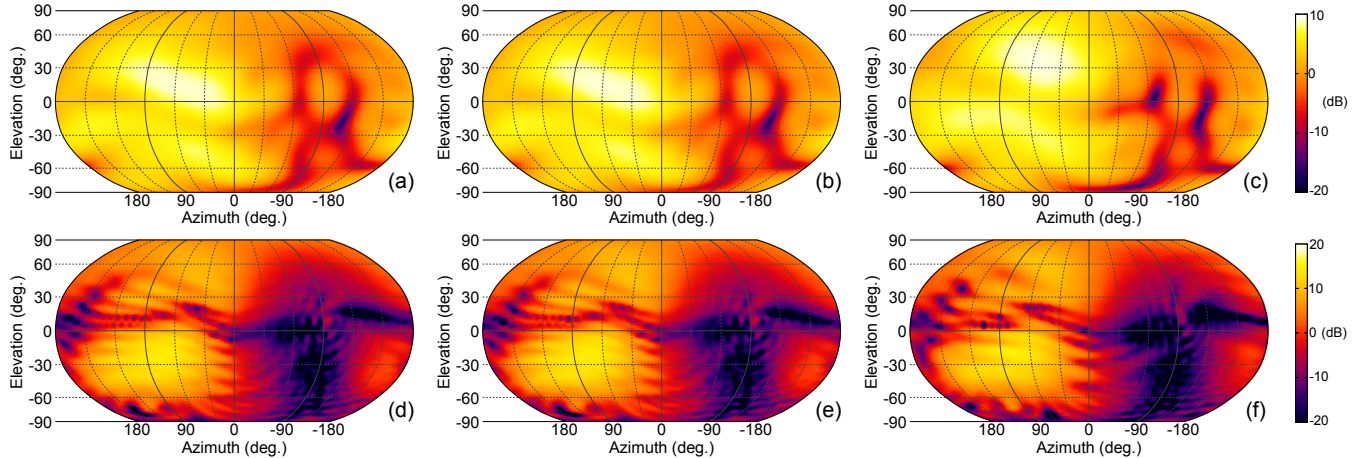


Fig. 5: SFRS plots for S_2 (a,d); $S_{12_{all}}$ (b,e); and $S_{12_{ear-only}}$ (c,f) are shown at two frequencies, 2 kHz (top row) and 10 kHz (bottom row).

to obtain $S_{12_{ear-only}}$.

In order to obtain the HRIRs corresponding to the six surface meshes (S_1 , S_2 , $S_{12_{ear-only}}$, $S_{12_{all}}$, $S_{21_{ear-only}}$, $S_{21_{all}}$) we apply FM-BEM simulations. In this work we used the Coustyx software by Ansol. The simulations were performed by the FM-BEM solver using the Burton-Miller Boundary Integral Equation (BIE) method. Using the acoustic reciprocity principle, a single simulation is used to determine all of the HRIRs in one go by placing a source on a surface mesh element that forms part of the blocked ear canal and then setting a uniform normal velocity boundary condition on this surface element. A post-processing step was used to refine the meshes prior to the FM-BEM simulation using the open-source software ACVD. The criteria the meshes need to meet during the mesh refinement are described in [6].

3. RESULTS

We now compare the FM-BEM simulated HRIR data for S_2 , $S_{12_{ear-only}}$, $S_{12_{all}}$. In order to make these comparisons we plot the spatial frequency response surfaces (SFRS) corresponding to the HRTF data. An SFRS plot (see [13] for details) shows the magnitude gain of the HRTF for a single frequency as a function of direction in space. Fig.5 shows the SFRS plots for S_2 , $S_{12_{ear-only}}$, and $S_{12_{all}}$ at 2 kHz and 10 kHz. The SFRS plots for S_2 and $S_{12_{all}}$ are pretty much identical, while the SFRS plot for $S_{12_{ear-only}}$ shows differences that can be attributed to the different torso and head. The spatial correlation between the SFRS's for S_2 and $S_{12_{all}}$ and between the SFRS's for S_2 and $S_{12_{ear-only}}$ was calculated as a function of frequency and are shown in Fig 6. Morphological differences in the torso and head causes the spatial correlation to dip around 2 kHz and somewhat surprisingly around 9 kHz.

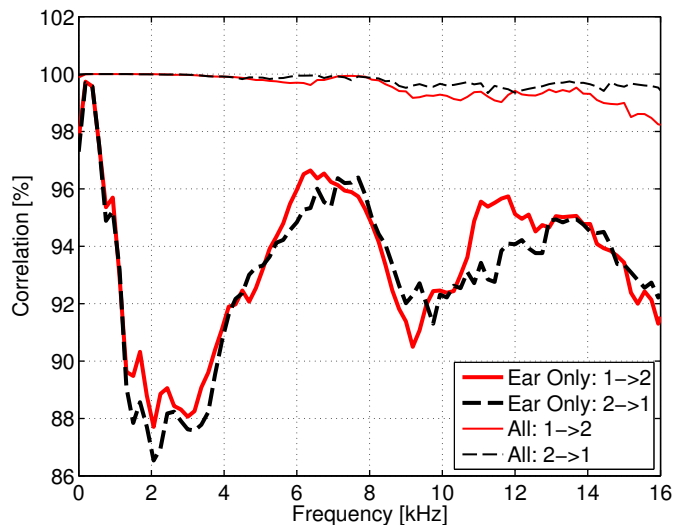


Fig. 6: The spatial correlation between various SFRS's are shown as a function of frequency. The spatial correlation is shown for the following pairing: (S_2 and $S_{12_{ear-only}}$) and (S_2 and $S_{12_{all}}$) – solid line; (S_1 and $S_{21_{ear-only}}$) and (S_1 and $S_{21_{all}}$) – dotted line.

4. CONCLUSIONS

In this paper we have demonstrated the first application and combination of the tools of LDDMM and FM-BEM to gain insights into binaural acoustics. We have shown how the tools can be applied to examine the classical question of “listening through another individual’s outer ear.” LDDMM provides a powerful and flexible tool to study, characterize and manipulate ear shapes. In future work, we will statistically characterize the distribution of torso, head and ear shapes and their relationship to changes in binaural acoustics.

5. REFERENCES

- [1] A.I. Tew, C.T. Hetherington, and J. Thorpe, “Morphoacoustic perturbation analysis,” in *Proceedings of the Joint meeting of the 11th Congrès Français d’Acoustique and the 2012 Annual Meeting of the Institute of Acoustics from UK*, Nantes, France, 2012, pp. 867–872.
- [2] C.T. Jin, P. Leong, J. Leung, A. Corderoy, and S. Carlile, “Enabling individualized virtual auditory space using morphological measurements,” in *Proceedings of the First IEEE Pacific-Rim Conference on Multimedia (2000 International Symposium on Multimedia Information Processing)*, 2000, pp. 235–238.
- [3] D.N. Zotkin, J. Hwang, R. Duraiswaini, and L.S. Davis, “Hrtf personalization using anthropometric measurements,” in *Proceedings of the WASPAA 2003*, 2003, pp. 157–160.
- [4] P. Mokhtari, H. Takemoto, R. Nishimura, and H. Kato, “Pinna sensitivity patterns reveal reflecting and diffracting surfaces that generate the first spectral notch in the front median plane,” in *Proceedings of the ICASSP 2011*, 2011, pp. 2408–2411.
- [5] N. A. Gumerov, A.E. O’Donovan, R. Duraiswami, and D.N. Zotkin, “Computation of the head-related transfer function via the fast multipole accelerated boundary element method and its spherical harmonic representation,” *Journal of the Acoust. Soc. of America*, vol. 127, no. 1, pp. 370–386, 2010.
- [6] C.T. Jin, A. Tew, P. Guillon, N. Epain, R. Zolfaghari, A. van Schaik, C. Hetherington, and J. Thorpe, “Creating the sydney york morphological and acoustic recordings of ears database,” *IEEE Transactions on Multimedia*, 2013.
- [7] Y. Kahana and P. A. Nelson, “Boundary element simulations of the transfer function of human heads and baffled pinnae using accurate geometric models,” *Journal of Sound and Vibration*, vol. 300, no. 3, pp. 552–579, 2007.
- [8] S.C. Joshi and M.I. Miller, “Landmark matching via large deformation diffeomorphisms,” *IEEE Transactions on Image Processing*, vol. 9, no. 8, pp. 1357–1370, 2000.
- [9] M.F. Beg, M.I. Miller, A. Trouvé, and L. Younes, “Computing large deformation metric mappings via geodesic flows of diffeomorphisms,” *International Journal of Computer Vision*, vol. 61, no. 2, pp. 139–157, 2005.
- [10] J. Glaunès, A. Qiu, M.I. Miller, and L. Younes, “Large deformation diffeomorphic metric curve mapping,” *International Journal of Computer Vision*, vol. 80, pp. 317–336, 2008.
- [11] M. Vaillant and J. Glaunès, “Surface matching via currents,” in *Information Processing in Medical Imaging*, G.E. Christensen and M. Sonka, Eds., vol. 3565 of *Lecture Notes in Computer Science*, pp. 381–392. Springer Berlin Heidelberg, 2005.
- [12] M. Vaillant, A. Qiu, J. Glaunès, and M.I. Miller, “Diffeomorphic metric surface mapping in subregion of the superior temporal gyrus,” *NeuroImage*, vol. 34, no. 3, pp. 1149–1159, 2007.
- [13] C.I. Cheng and G.H. Wakefield, “Spatial frequency response surfaces: an alternative visualization tool for head-related transfer functions (hrtfs),” in *Proc. of the ICASSP 1999*, March 1999, vol. 2, pp. 961–964.